Remote Sensing of Environment 259 (2021) 112427

Contents lists available at ScienceDirect

Remote Sensing of Environment

journal homepage: www.elsevier.com/locate/rse

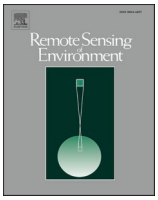

Mapping of wheat lodging susceptibility with synthetic aperture radar data

Sugandh Chauhan [a], Roshanak Darvishzadeh [a,*], Sander H. van Delden [b], Mirco Boschetti [c], Andrew Nelson [a]

[a] Faculty of Geo-information Science and Earth Observation (ITC), University of Twente, 7500AE Enschede, the Netherlands
[b] Horticulture and Product Physiology, Wageningen University, PO Box 16, 6700AA Wageningen, the Netherlands
[c] CNR-IREA, Institute for Electromagnetic Sensing of the Environment, National Research Council, 20133 Milan, Italy

ARTICLE INFO

Editor name: Jing M. Chen

Keywords:
Lodging susceptibility
Wheat
Remote sensing
Sentinel-1
RADARSAT-2
Safety factor
SAR

ABSTRACT

Crop lodging reduces yield quantity and grain quality of cereal crops. Understanding seasonal variation in crop lodging susceptibility enables lodging risk assessments and predictions of associated crop yield losses. We demonstrate a novel remote sensing-based approach, using sparse field observations and widely available synthetic aperture radar (SAR) satellite imagery, to map a safety factor against root lodging (SF_A) in wheat. SF_A quantifies the ability of the rooting system to support the self-weight moment of the whole plant and can be used as an indicator of in-season root lodging susceptibility. SAR satellite images, from Sentinel-1 and RADARSAT-2, were acquired synchronously with field measurements in Jolanda di Savoia, Ferrara, Italy during the 2018 winter wheat growing season. The field data included measurements from non-lodged (healthy) wheat such as plant height, height at the centre of gravity, self-weight moment of the whole plant, soil anchorage strength, SF_A and those from lodged wheat such as crop angle of inclination, lodged area and the point of plant failure (stem or root). Field measurements confirmed that SF_A decreased progressively through the season and was consistent with the observed lodging. Strong and significant correlations through the season were observed between SF_A and SAR satellite image metrics. The validated regression models showed a strong relationship between field-measured SF_A and the metrics from RADARSAT-2 ($R^2_{CV} = 0.84$, $RMSE_{CV} = 0.54$) and Sentinel-1 data ($R^2_{CV} = 0.73$, $RMSE_{CV} = 0.59$). However, it is possible that the relationship between SF_A and SAR parameters is confounded by the variations in crop biomass, which is highly correlated with SF_A ($r = -0.71$, $p < 0.0001$). Our study, for the first time, demonstrates the use of remote sensing SAR data for lodging susceptibility assessment. Current and planned satellite platforms have the potential for large scale, operational assessment of lodging susceptibility in cereal crops.

1. Introduction

Crop lodging, which is the permanent displacement of the crop's stem from its vertical position (Pinthus, 1974), can cause severe yield reductions by up to 75% in cereals (Berry and Spink, 2012). Lodging is also associated with delayed harvest, increased drying costs, deterioration in grain quality and increased susceptibility to mycotoxins (Fischer and Stapper, 1987). Accurate spatio-temporal information about crop lodging and its susceptibility during the growing season are critical for improving yield estimates, increasing productivity and targeting lodging control interventions.

Lodging is caused by either stem failure (stem lodging) or anchorage failure (root lodging) and the most probable form of lodging is governed by genetic, management and environmental factors (Berry et al., 2003a). For instance, high plant population density increases the susceptibility of root lodging over stem lodging, while the early application of nitrogen fertilizer may favour stem lodging (Berry et al., 2000). Root lodging is more predominant in wheat than stem lodging (Crook and Ennos, 1993). For example, an extensive study (Berry et al., 2003a) examining 15 winter wheat cultivars at three UK sites between 2000 and 2002 showed that root lodging varied between 2 and 47%, while stem lodging was observed in only 0–19% of the wheat cultivars.

Before we proceed, it is important to understand the conceptual differences between the two terms: susceptibility and risk. In the case of lodging, susceptibility means the degree to which the crop is prone to lodging. It captures the fact that the host (the plant) reacts variably to lodging, some plants do better than others even if the exposure to a certain external factor is the same. Heavy rain increases the risk of

* Corresponding author.
E-mail address: r.darvish@utwente.nl (R. Darvishzadeh).

https://doi.org/10.1016/j.rse.2021.112427
Received 21 July 2020; Received in revised form 25 March 2021; Accepted 31 March 2021
Available online 6 April 2021
0034-4257/© 2021 The Authors. Published by Elsevier Inc. This is an open access article under the CC BY license (http://creativecommons.org/licenses/by/4.0/).

lodging, but the amount and severity of lodging that occurs will be (partially) determined by how susceptible each plant is to lodging. The cultivar, environment, management practices and their complex interactions, strongly influence these factors due to their effects on the crop structure (Berry et al., 2004). A study of all these factors together can form part of a comprehensive lodging risk assessment.

Conventional measures to assess lodging susceptibility are primarily based on visual inspection of the crop (Caldicott and Nuttall, 1979). Visual assessments are sparse, subjective, time-consuming and costly (Bock et al., 2010). Alternatively, mathematical models based on the underlying physics of plant structure might be used to assess lodging (Berry et al., 2003b). Although these mechanistic models facilitate an in-depth understanding of the lodging phenomenon, the detailed measurements required to parameterize these models make them input-intensive; therefore, mechanistic models are challenging to apply on a large scale. In this regard, some efforts have been made to develop "simple" lodging susceptibility indicators (Crook and Ennos, 1995, 1993).

A safety factor against root lodging (SF_A) has been conceptualized as a "simple" indicator of root lodging susceptibility (Crook and Ennos, 1994). The SF_A is the ratio between the root anchorage strength (S_A) and the self-weight moment of the whole plant (M_P) generated by all the aerial parts, i.e. stems, leaves and heads (Fig. 1). SF_A correlates well with lodging in the field, with lodging resistant cultivars having greater SF_A (>1) than susceptible cultivars (≤1) (Crook and Ennos, 1994, 1993; van Delden et al., 2010). Accurate information about the variability of SF_A and its distribution can enable assessment of root lodging susceptibility and help mitigate lodging impacts (e.g., lodging controls).

Satellite-based remote sensing (RS) data, with its ability to cover large geographic areas with repeated observations, offer a promising alternative for lodging monitoring and susceptibility assessment. So far in the context of lodging assessment using satellite RS data, only three research avenues have been investigated: i) discrimination between lodged and non-lodged areas (Chen et al., 2016), ii) detection of when lodging occurs (Chauhan et al., 2020c), and iii) classification of lodging severity (Chauhan et al., 2020a). These studies diagnose lodging events after they have occurred and emphasize the need for precise and timely Earth observation data for improving lodging assessment. These studies have emphasized that cloud contamination in optical RS data can substantially decrease the number of suitable observations over a region of interest. At the same time, synthetic aperture radar (SAR) sensors can create gap-free datasets for continuous lodging monitoring.

A sound theoretical basis for RS-based lodging susceptibility assessment and the underlying estimation of lodging susceptibility indicators is still missing. Seasonal assessment of lodging susceptibility is important in many aspects - for optimal resource utilization in risk-prone areas, effective decision-making in selecting remedial measures (e.g., nitrogen or plant growth regulator application at critical growth stages), for decreasing crop production costs and reducing the impact on crop yield and grain quality.

This study aims to address this gap and contribute to future lodging risk prediction studies by estimating SF_A as a simple measure of in-season root lodging susceptibility using SAR data. For seasonal susceptibility, we assess the actual plant condition that can influence lodging due to the interaction between genetic, environment and management factors that can amplify or reduce the inherent propensity of different cultivars to lodging. In this study, we compare the performance of RS-based metrics derived from multi-temporal Sentinel-1 (dual-polarized) and RADARSAT-2 (quad-polarized) datasets representing state-of-the-art observational platforms for agricultural monitoring. We also discuss the performance of field-measured SF_A in detecting root lodging susceptibility throughout the growing season and analyze the lodging susceptibility of nine different cultivars.

2. Materials and methods

2.1. Study area description

The study was carried out in the Bonifiche Ferraresi farm (central coordinates 44°52′59″N, 11°58′48″E), in Jolanda di Savoia, Ferrara, Italy (Fig. 2a, b). Bonifiche Ferraresi is one of the largest farm holdings (>6000 ha of land) and agri-food companies in Italy, covering an area of approximately 3850 ha in the Emilia Romagna region of Jolanda di Savoia municipality. The Jolanda estate is a major agricultural area

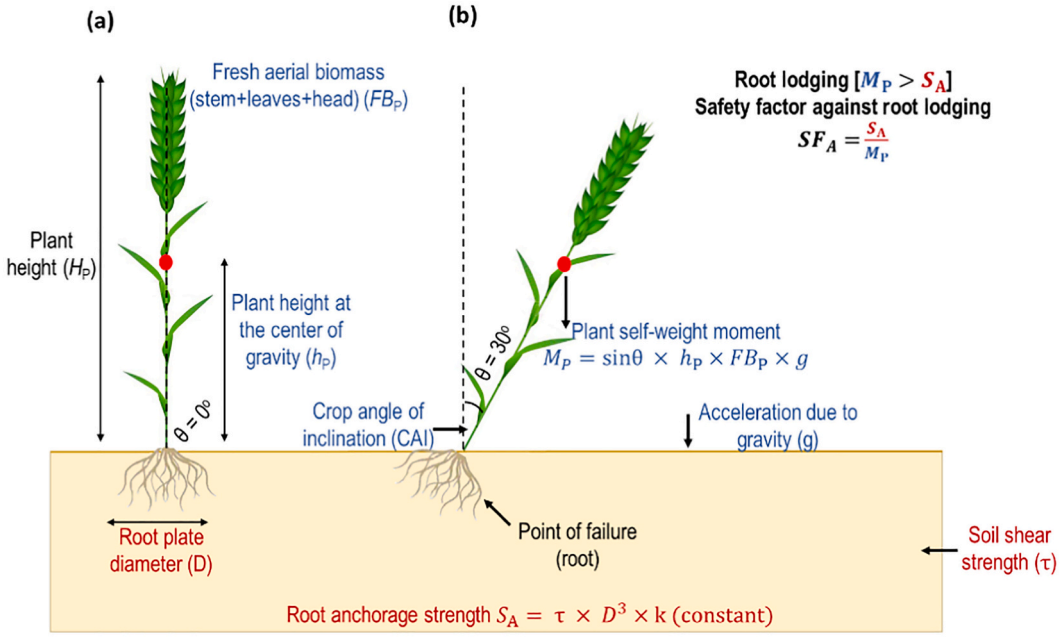

Fig. 1. Schematic diagram of the safety factor against root lodging. Crop and soil parameters are governing the safety factor against root lodging (SF_A) for two scenarios (A) healthy/non-lodged wheat with θ = 0° and (B) root lodged wheat with θ = 30°. An SF_A is a ratio of the plant self-weight moment (M_P, N-m) and root anchorage strength (S_A, N-m). M_P is a function of crop angle of inclination (CAI, θ°), height at the center of gravity (h_P, m), fresh aerial biomass (FB_P, kg) and acceleration due to gravity (g, N kg^{-1}). S_A is a function of root plate diameter (D), soil shear strength (τ) and a dimensionless constant (k).

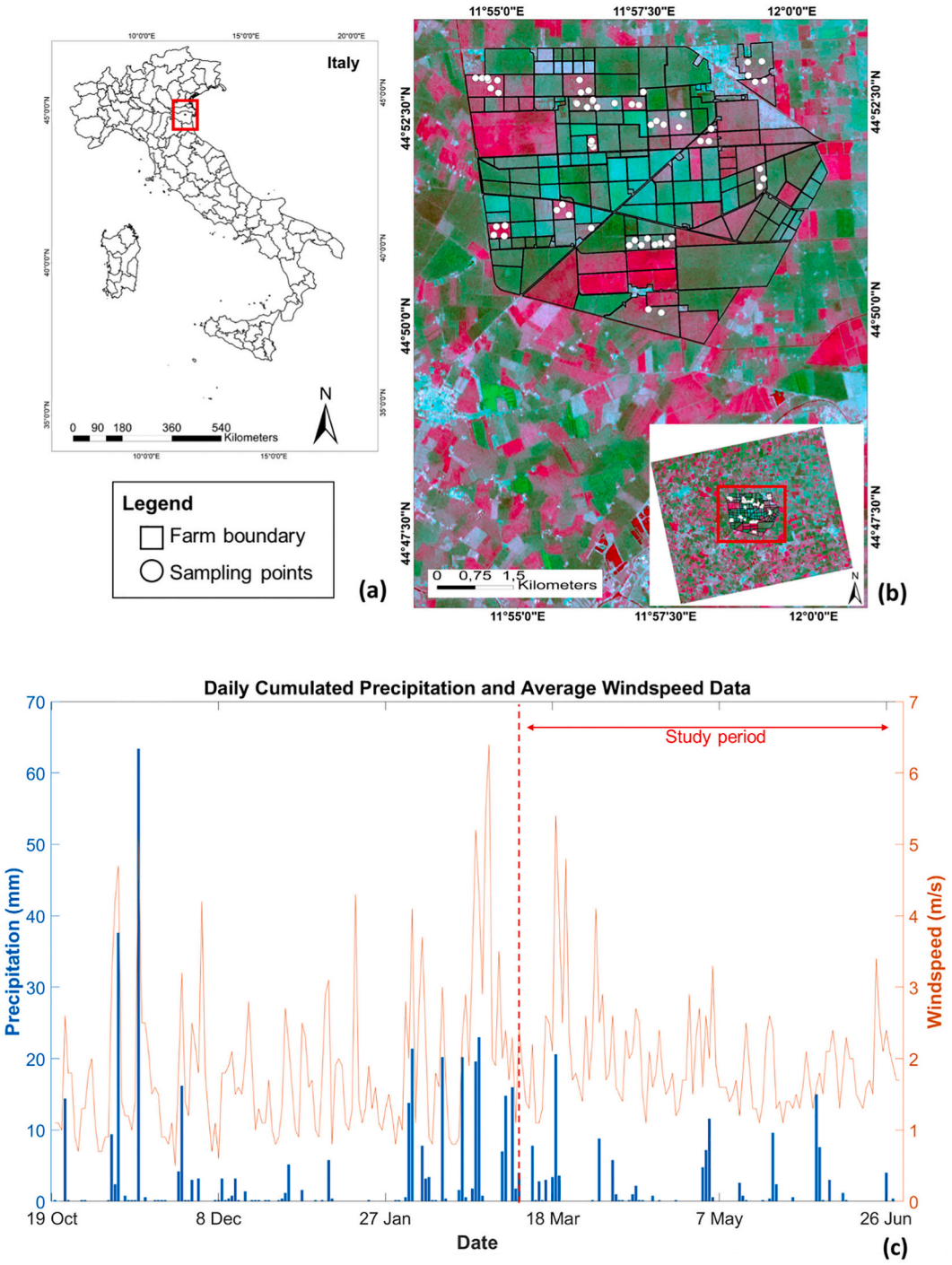

Fig. 2. Study area description. (a) The red polygon is the location of the study region in Northern Italy. Also shown is (b) a Sentinel-1 RGB composite (R: VH/VV, G: VV, B: VH) of a scene acquired on April 19, 2018 containing the study area (Bonifiche Ferraresi farm, a red polygon in the lower-left map) overlaid with the farm boundary (black outline) and the sampled plots (white dots) over the wheat sown fields. (c) illustrates the distribution of daily cumulated precipitation (mm) and daily average wind speed (m/s) at 10 m from the ground during the winter wheat growing season from October 19 to June 30, 2018. The period of this ranges from March 14 to June 30, 2018. (For interpretation of the references to colour in this figure legend, the reader is referred to the web version of this article.)

where wheat (*Triticum aestivum*) is grown as a staple crop in rotation with others in consecutive years. Soils are mainly clayey and silty in texture and the climate is warm and temperate. In the 2017–18 wheat season, wheat was sown in approximately 600 ha area between October 21–November 4, 2017 and was harvested by the end of June 2018. Several cultivars with a wide range of lodging susceptibility scores (LSS), as reported by seeding company's technical sheet and local expert score system, were sown in the study area: PR22D66 (LSS: 1.5), Marco Aurelio (2.5), Rebelde (3), Massmio Meridio (3), Claudio (4), Monastir (5), Odisseo (6.5), Giorgione (7) and Senatore Capelli (9). The LSS (ranging from 0 to 9) indicates the susceptibility of a cultivar to lodging with a LSS of 9 depicting maximum lodging susceptibility. It is important to notice how Senatore Capelli, an old variety from the 1930's cultivated mainly for its high grain quality, shows an extremely high susceptibility to lodging. During the wheat growing season of 2017–18, the daily cumulated precipitation and average wind speed, as measured from a

local automatic weather station, ranged between 0 and 65 mm and 0.5–6.4 m/s, respectively (Fig. 2c).

2.2. Experimental design and field measurements

We used stratified random sampling with information derived from six raster layers (sowing date, soil pH, soil type, elevation, seed density and crop cultivar) to obtain spatially distributed sampling points and represent the heterogeneity of the research area. We selected a total of 61 plots (size 60 × 60 m per plot) on the basis of a *t*-test based power analysis (with a power of 0.95). These plots are overlaid on the satellite image in Fig. 2b. To capture the variability of crop growth in each plot, we selected three subplots (2 × 2 m) and averaged the readings to get plot-level measurements. We revisited each plot three times in 2018 between March 14 and June 30 to measure crop biophysical and structural variables: i) we took measurements for plant height (H_P in m); root anchorage strength (S_A in N-m); plant height at the center of gravity (h_P in m); self-weight moment of the whole plant (M_P in N-m); fresh aerial biomass (FB_P in kg) and determined the crop phenological stage using the Biologische Bundesanstalt, Bundessortenamt and CHemical industry (BBCH) scale (Bleiholder et al., 2001).

During the entire duration of the field campaign, 30 plots were found to be lodged at the end of the season while the others remained healthy until the end of the season. To see if SF_A can actually be used as an indicator of root lodging susceptibility in wheat (and to predict the overall lodging risk later in the season), it was first important to analyze how field measured SF_A values vary in both lodged and non-lodged scenarios. Therefore, the field measurements were used for two different purposes as follows:

(i) First, we demonstrated how field measured SF_A vary with lodging susceptibility scores (LSS) and observed lodging in the field. The results of this preliminary analysis would establish if SF_A in fact, could be used as an indicator to map lodging susceptibility.
(ii) Secondly, we investigated the potential of SAR derived metrics to estimate SF_A, through regression analysis. For the model development and validation to predict SF_A, we only used the samples from healthy wheat (non-lodged wheat). The rationale behind using only healthy samples to predict SF_A is that SF_A should be able to indicate the susceptibility of the healthy samples to lodge in the future early in the season (when the plants are still healthy) or even at later growth stages. Moreover, lodged plants have a different plant morphology and physiology hindering a proper measurement of SF_A. So once the plants are lodged the SF_A measurements are no longer helpful as they cannot be used as a proper a priori measure to assess the susceptibility of the event.

Overall, the sampled observations covered four major crop phenological stages – stem elongation, booting, flowering, and milking (Fig. 3).

The field measurement protocol was as follows: first, we recorded plant height (H_P), defined as the distance from the soil surface to the tip of the head of the longest tiller; then S_A was measured by subjecting the plants to lodging using a custom-built, handheld lodging meter (Fig. 4). The lodging meter was built using a sensitive digital torque screwdriver (reading up to 6 N-m with 0.001 N-m intervals; Mecmesin Ltd., UK) fitted with an integrated tiller holding cup, a lodging arm and an outer casing with four spikes similar to (Crook and Ennos, 2000; van Delden et al., 2010) (Fig. 4a). To estimate S_A the following steps were taken: i) Stubbles were created by cutting all stems at 10 cm above soil level, the upper mass was preserved to measure (h_P) and fresh aerial biomass (FB_P). ii) To make the stubbles behave like a rigid beam and avoid bending, lightweight hollow metalcore was inserted in the middle of the stubbles and the stubble-pin combination was tied together with a fastener (Fig. 4b). iii) The lodging meter was inserted into the soil such that the setup could deliver a rotational force around the base of the plant stem (Fig. 4b). iv) Using the lodging meter, the stubble-pin combination was pushed over to create different angles of inclination (AIs) from the vertical, i.e., 10°, 20°, 30°, 40°, 45° and 60° and at each angle, we recorded the maximum root resistance, i.e., root anchorage strength (S_A) (Fig. 4c). The moment of failure was identified by reading the

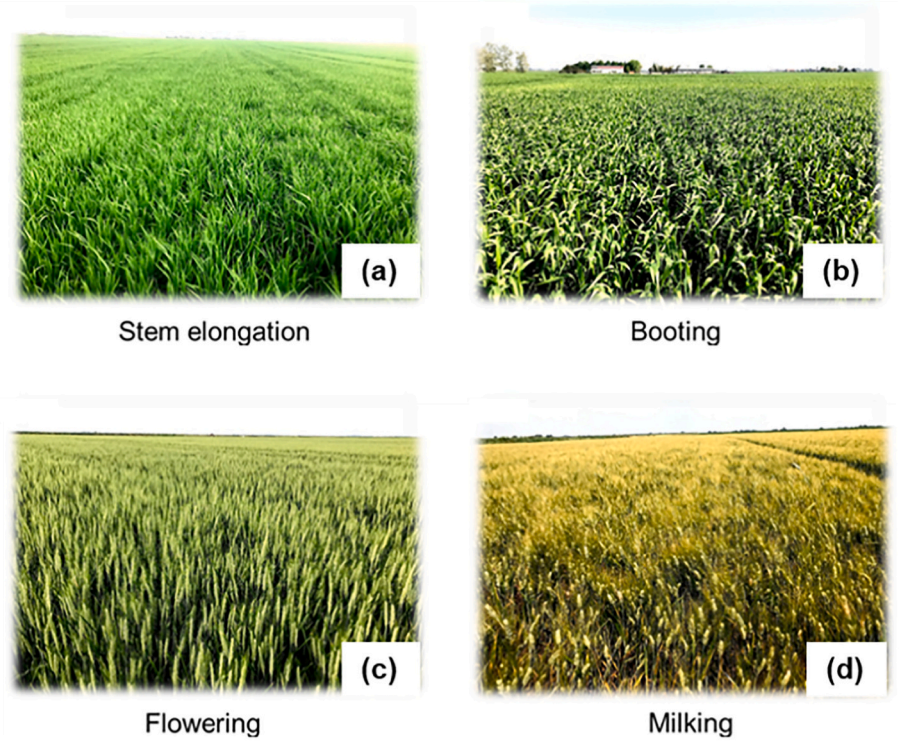

Fig. 3. Field photographs of wheat in different phenological stages: (a) stem elongation, (b) booting, (c) flowering and (d) milking.

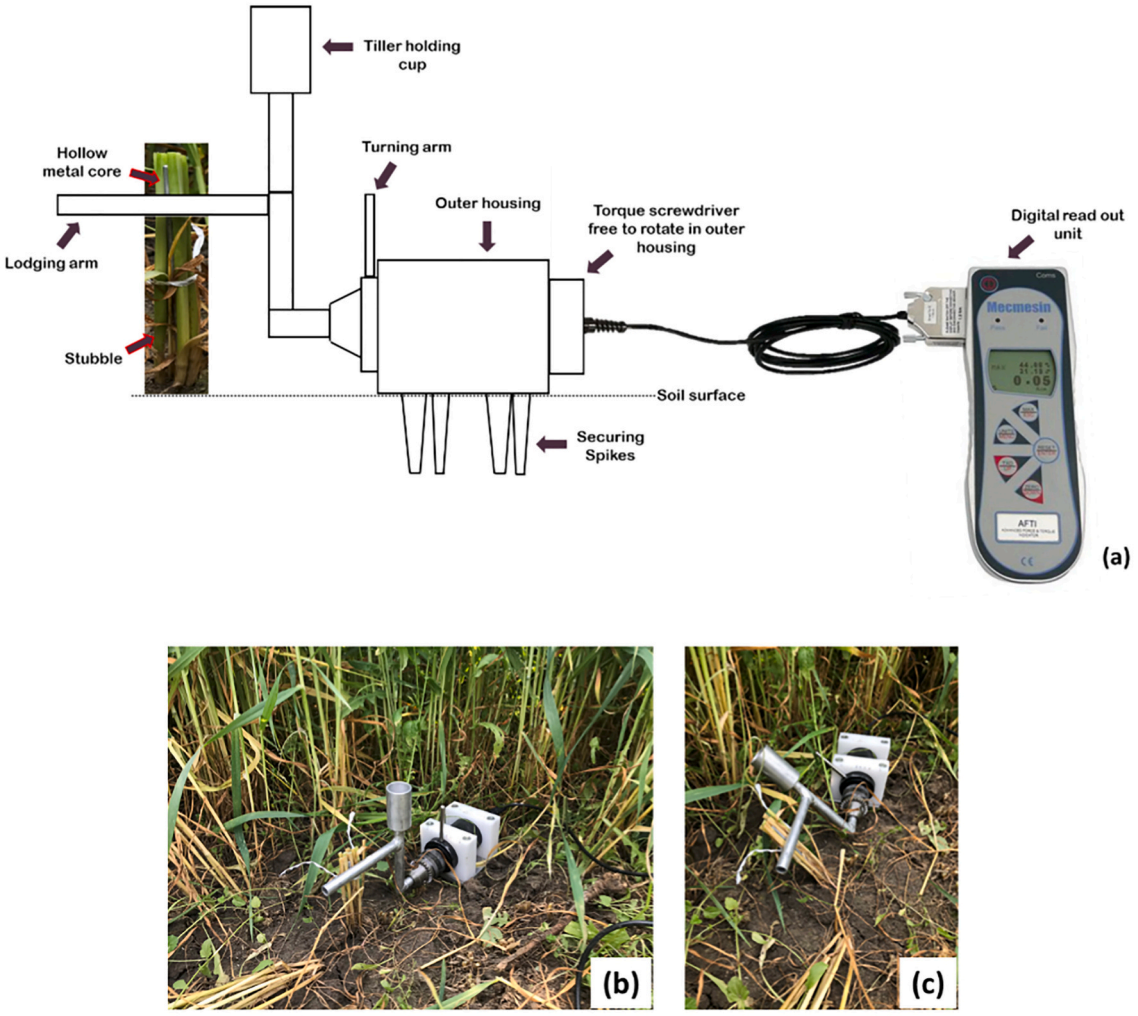

Fig. 4. Basic layout of the lodging meter and its demonstration in the field. (a) Schematic illustration of the lodging meter connected with a portable digital unit, (b) shows the setup of the lodging meter in the soil. The stubble (stem base cut 10 cm from the soil surface) with a hollow metal core inserted in between and tied with a fastener is shown. The lodging meter is placed level with the soil at a distance such that the lodging arm touches the stubble-pin combination and (c) illustrates the procedure to measure the root anchorage strength at different crop angles of inclination.

maximal resistance at the angle of inclination at which the roots break. Crown root breakage can be identified on the display by a sudden drop in resistance while moving the lodging meter. It was sometimes even audible; one can hear a click.

We ensured that the neighboring plants did not interfere with these measurements and the readings were corrected for the self-weight moment of the stubble-pin combination and the pushing device. We then cut off the stubble at soil level and tied the stubble together with the remaining section of the plant (with lightweight tape) and measured the h_P of the whole plant using a balancing method. We balanced the plant on a thin (3 mm), smooth metal tube to find the balance point of the whole plant, while the leaves and ears were still attached. h_P was defined as the distance between the balance point and the stem base. Then FB_P was measured using a high-precision digital scale. Lastly, we calculated the self-weight moment of the whole plant (M_P in N-m) and the safety factor against root lodging (SF_A) using Eq. (1) and Eq. (2) (Crook and Ennos, 1994), respectively.

$$M_P = sin\theta \times h_P \times FB_P \times g \quad (1)$$

$$SF_A = \frac{S_A}{M_P} \quad (2)$$

where M_P (N-m) is the self-weight moment of the whole plant at 10^o, 20^o, 30^o, 40^o, 45^o, 60^o from the vertical, h_P (m) is the plant height at the center of gravity, FB_P (kg) is the fresh aerial biomass, g (N kg^{-1}) is the acceleration due to gravity; g is ~9.81 N kg^{-1}, SF_A is the safety factor against root lodging and S_A (N-m) is the maximum root anchorage strength. The summary statistics of the field measured variables are in Table 1.

Table 1
Summary statistics of field measurements. A statistical summary (mean, minimum, maximum, standard deviation and coefficient of variation) of the field measurements are provided for non-lodged (healthy) wheat across the wheat-growing period ($n = 90$). *CAI* is the crop angle of inclination. The measurements were taken from 61 plots with different wheat cultivars.

Parameter	Mean	Min.	Max.	Std. Dev.	COV
Plant height (m)	0.50	0.20	1.01	0.27	0.54
Height at the center of gravity (m)	0.21	0.04	0.65	0.16	0.79
Fresh biomass (kg m^{-2})	0.33	0.05	1.01	0.22	0.65
Self-weight moment of the whole plant (N-m) (CAI = 30^o)	0.46	0.013	2.57	0.55	1.21
Root anchorage strength (N-m) (CAI = 30^o)	0.18	0.013	1.80	0.23	1.34
Safety factors (CAI = 30^o)	0.98	0.056	2.90	0.79	0.81

2.3. Remote sensing data acquisition

We acquired remote sensing images synchronously with the field observations (Table A1). We downloaded ten Sentinel-1A/B (in Interferometric Wide swath mode) images in ascending mode between March 14 and June 30, 2018 via the Copernicus Open Access Hub. The Interferometric Wide swath mode provides data in dual-polarization mode (VV: Vertical-Vertical and VH: Vertical-Horizontal). We acquired the images in both ground range detected (GRD) and single look complex (SLC) formats to facilitate the extraction of backscattering coefficients and polarimetric/coherence parameters, respectively. The incidence angle over the surveyed study site ranged between 39.7° to 40.4°. The spatial resolution was resampled to 15 m.

We also obtained five SLC RADARSAT-2 images in fine quad-polarization mode through the Canadian Science and Operational Applications Research Program (SOAR). We selected the fine-polarization mode for its high spatial resolution and quad-polarized configuration that permits the derivation of various polarimetric parameters. We procured the images in different beam modes with incidence angles ranging from 26.9–28.7° to 40.2–41.6°. The nominal spatial resolution of the images was resampled to 10 m.

2.4. Remote sensing data processing

2.4.1. Sentinel-1

We pre-processed Sentinel-1 images in SARscape 5.5 to extract backscattering coefficients ($\sigma^o\sigma^o$) and coherence (μ^o) metrics and carried out polarimetric decomposition in SNAP 6.0. After applying the precise orbit correction on the GRD images, we extracted the backscattering coefficients (σ^o_{VH}, σ^o_{VV}, $\sigma^o_{VH/VV}$) in dB units using the methodology outlined by Nelson et al. (2014). In addition, we also applied orientation angle correction to remove the azimuth slope variations. The Radar Vegetation Index (RVI) for dual-pol data proposed by Charbonneau et al. (2005) was later derived using Eq. (3):

$$RVI = \frac{4\sigma^o_{VH}}{(\sigma^o_{VH} + \sigma^o_{VV})} \quad (3)$$

where σ^o_{VH} and σ^o_{VV} are the backscattering coefficients (in dB) in VH and VV polarizations.

We used the phase processing coherence module of SARscape to generate geocoded coherence maps. Unlike SAR, which utilizes the amplitude information of a complex SAR signal, InSAR utilizes phase information to calculate interferometric coherence (that includes both, the interferometric correlation coefficient and interferometric phase). Coherence is a function of the change in phase or amplitude of an image pixel and is defined as the systemic spatial or scene de-correlation that occurs between two acquired dates. These changes in the backscatter can be due to differences in dielectric properties (e.g. wet or dry soil), due to natural processes (e.g. growth of crop) or abrupt changes (e.g. crop harvesting or lodging) all of which can cause coherence loss. γ is formulated as the amplitude of the complex correlation coefficient between two SAR scenes,

$$\gamma = \frac{\left|\langle s_1 s_2^* \rangle\right|}{\sqrt{(\langle s_1 s_1^* \rangle \langle s_2 s_2^* \rangle)}} \quad 0 \le \gamma \le 1 \quad (4)$$

where, γ is the interferometric coherence, |..| represents the absolute values, ⟨..⟩ denotes the averaging operation, * is the complex conjugate product, and s_1 and s_2 are the complex pixel values from the two image dates (Touzi et al., 1999). The processing steps for coherence estimation include i) Orbit file and orientation angle correction, (ii) interferogram generation. This step resamples the slave image onto the geometry of the master image, applies multilooking and generates a coregistered output. The coregistration accuracy was improved (in the order of 1/1000th of a pixel) using an external DEM (10 m resolution) as an additional input and spectral diversity techniques, iii) interferogram flattening using the external DEM and topographic phase removal, iv) adaptive phase filtering to reduce noise and coherence estimation, v) geocoding.

SARscape, based on the master input data resolution, suggests the azimuth and range multi-looking factors. The multi-looking factors of 4 (looks in range direction) × 1 (looks in azimuth direction), leading to the pixel size of 13.27 m × 13.8 m, was used for Sentinel-1 to increase the signal-to-noise ratio (SNR) of the interferograms and obtain squared pixels. A similar approach was also used by Darvishi et al. (2018) and Khabbazan et al. (2019) for coherence estimation. We also filtered the interferograms for visual inspection, and to identify fringe patterns and coherence estimation using a Goldstein filter. Additionally, we used the SARscape Sentinel-1 SLC data processing guidelines, which recommends setting the cartographic grid size for Sentinel-1 SLC data as 15 m. The resampling parameters were estimated from the orbital data and by exploiting cross-correlation and coherence maximization techniques. In order to achieve the lowest temporal baseline (six days), we estimated γ between every adjacent image pair (e.g. between date 1 and date 2; between date 2 and date 3; and so on). The coherence (γ) reported for a given date indicates the coherence between the image on that date (or the closest available later date to the field data, i.e. N) and its predecessor, i.e. N-1. The in-situ observations were matched to the coherence image pairs based on the N image date. The coherence value $\gamma_{N\text{-}1,N}$ was assigned to the in-situ observation if the date of the latter was either close to N or if it fell between N-1 and N.

We also applied a dual-pol *H*/α/*A* polarimetric decomposition to the SLC images using the Graph Builder and Batch processing capabilities of SNAP. The processing chain consisted of six steps: i) orbit file correction, ii) Terrain Observation with Progressive Scan (TOPS) Split to extract the sub-swath with our region of interest, iii) radiometric calibration, iv) TOPS Deburst to remove the demarcation zones between the bursts, v) Refined Lee polarimetric speckle filter with 5 × 5 window, and vi) *H*/α/*A* decomposition to produce entropy (*H*), alpha angle (α) and anisotropy (*A*) parameters. *H*/α/A decomposition, proposed by (Cloude and Pottier, 1996), is an eigenvector-eigenvalue based decomposition. *H* [0,1] accounts for the heterogeneity of the scattering, α [0,90°] indicates the type of scattering (surface, double-bounce or volume) and *A* provides information on the relative importance of the secondary mechanisms occurring in the pixel. The anisotropy may reach 0 value for a dominant scattering mechanism. We processed all the SLC images in a batch mode to produce the decomposed outputs and then co-registered and terrain corrected them. Thus, for each Sentinel-1 acquisition, we computed nine metrics: i) $\sigma^o_{VH}\sigma^o_{VH}$, ii) σ^o_{VV}, iii) $\sigma^o_{VH/VV}$, iv) RVI, v) $\gamma_{VH}\gamma_{VH}$ vi) $\gamma_{VV}\gamma_{VV}$, vii) *H*, viii) α and ix) *A*.

2.4.2. RADARSAT-2

Similar to Sentinel-1 data, we pre-processed RADARSAT-2 images in SARscape 5.5 to extract σ^o and carried out polarimetric processing in SNAP 6.0. We used definitive orbit files obtained from the MacDonald Dettwiler Associates Ltd. FTP repository to update the orbital information in the RADARSAT-2 images. We used the approach outlined in Nelson et al. (2014) to get normalized σ^o σ^ovalues (dB). The backscatter was normalized for the incidence angle induced variations using the cosine law of incidence angle (Nelson et al., 2014), and an orientation angle correction was applied to remove the variations due to azimuth slope (Souissi and Ouarzeddine, 2016). For polarimetric decomposition, we applied a Refined Lee polarimetric speckle filter (5 × 5 window) on the calibrated images to eliminate speckle noise while preserving the complex information. We then used different polarimetric decomposition methods: i) Sinclair decomposition, ii) Pauli decomposition, iii) *H*/α/*A* decomposition, iv) Freeman-Durden decomposition, v) Yamaguchi decomposition, vi) Cloude decomposition, vii) Touzi decomposition and viii) Van Zyl decomposition to decompose the radar scattering matrix into components that could be physically interpreted in terms of the scattering mechanisms. The detailed description of these methods can be found in Chauhan et al. (2020b).

In addition to the decomposition parameters, we also computed

simple SAR polarimetric parameters such as span, biomass index, RVI, pedestal height, volume scattering index, canopy scattering index, radar forest degradation index, co-pol (σ^o_{HH}/ σ^o_{VV}) ratio and cross-pol (σ^o_{HH}/ σ^o_{HV}) ratio from the radiometrically calibrated images. The detailed description of these parameters can be found in Chauhan et al. (2020b). Lastly, we co-registered and geocoded the images and extracted 39 metrics (Table A3) from them.

2.5. Statistical analysis

In this study, we performed two different kinds of statistical analyses: (i) Pearson correlation coefficient analysis aimed at understanding the correlation between the predictors, i.e. remote sensing metrics derived from Sentinel-1 and RADARSAT-2 data (Table A2, A3) and the safety factor against root lodging (SF_A); and (ii) an Extreme Gradient Boosted Tree Ensemble (XGB) for regression to estimate SF_A using the remote sensing predictors. Pearson correlation coefficient, also referred to as Pearson's r [−1,1], is a statistic to measure the linear correlation between the two variables. It is an established way to provide insights into the black-box machine learning algorithms as it can indicate the relative performances of different predictor variables.

XGB is a non-parametric regularized extension of traditional boosting techniques (Chen and Guestrin, 2016). It iteratively applies tree-based approximation to varying gradient descent by predicting a new membership value after each iteration to minimize the overall loss (Torres-Barrán et al., 2019). The overall loss is depicted by a cost function that measures the difference between the observed and the predicted output from the model. Boosting works on the principle of the ensemble, which means that a set of weak learners are combined to improve the prediction accuracy. This is achieved by weighing the outcome of the model at an instant *t* based on the outcome of the previous model at instant *t-1* and capitalizing on the error. XGB simplifies the objective functions by combining the training loss and regularization terms to prevent overfitting (Zhang et al., 2020). The training loss measures the predictive capability of the model with regard to the training data while the regularization term accounts for the model complexity. The aim is to develop a simple, yet predictive model and the tradeoff between the two is known as a bias-variance tradeoff.

In this study, we implemented an extreme gradient boosting tree ensemble regression model to estimate safety factor parameter using the XGBoost package in MATLAB in the partial least square toolbox v8.7 from Eigenvector Research, Inc., with the Multivariate Image Analysis toolbox v3.0 add-on (in MATLAB 2018b). We trained and cross-validated the models separately with the input metrics from Sentinel-1 and RADARSAT-2 data separately. The input metrics derived from each sensor data are mentioned in Table A2 and A3. We used a cross-validated grid-search to tune the hyperparameters and select the optimal parameter values to build the models. Thus, there were two nested levels of sub setting: one for fine-tuning the hyperparameters and select the optimal parameter values to the build the models and second for cross validating the models. We used $RMSE_{CV}$ as the evaluation measure of the model performance, with the model parameters yielding the lowest $RMSE_{CV}$ being chosen as the best performing model. We used a five-fold Venetian blinds cross-validation procedure to divide the datasets into training and validation subsets. This method guarantees that both training and validation sets span across the entire data range (Allison et al., 2009). This involved dividing the datasets randomly into five subgroups, performing five iterations such that each subgroup could be used once as a validation set and giving an average output. We then used the final cross-validated models to generate SF_A maps of all the wheat fields in the study area. The methodological flowchart of the study is shown in Fig. 5.

3. Results

3.1. Temporal variation of field-measured parameters

Field measurements on biophysical and structural parameters (Table 1) of nine winter wheat (*Triticum aestivum*) cultivars were performed between March 14 (early stem elongation stage: BBCH 30) and June 23, 2018 (crop maturity: BBCH 99). We limit our interpretation of the temporal variation in field-measured parameters from non-lodged (healthy) wheat to four phenological stages: stem elongation (BBCH 30–39), booting (BBCH 40–49), flowering (BBCH 60–69), and milking

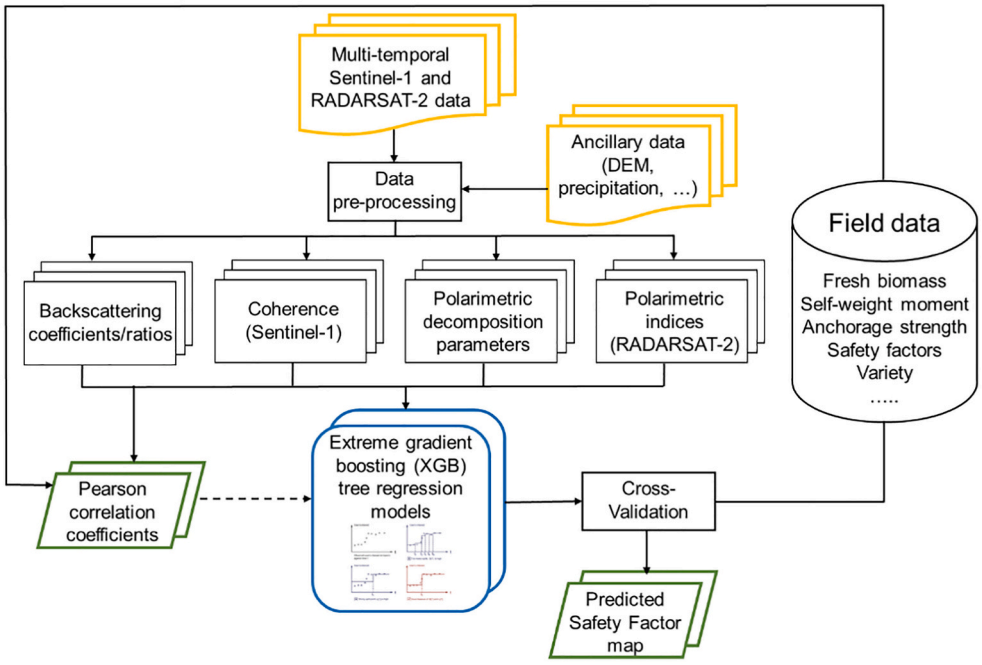

Fig. 5. Process flowchart for the estimation of safety factor against root lodging. The inputs are colour-coded in yellow, the model used is in blue, and primary/intermediate outputs are in green. The dashed line signifies that the output is used for interpretation. (For interpretation of the references to colour in this figure legend, the reader is referred to the web version of this article.)

(BBCH 70–77). Samples from later phenological stages (BBCH>80) were mostly lodged and were excluded from the analysis but were used for validating the performance of SF_A for assessing root lodging susceptibility.

Plant height (H_P) and height at the centre of gravity of the whole plant (h_P) (Fig. 6a) changed from a mean of 0.30 and 0.08 m during stem elongation stage to 0.86 and 0.49 m in the milking stage, respectively (Fig. 6a, b). They exhibited a similar pattern of change across the season and were found to correlate with each other positively ($r = 0.96$, $p < 0.001$). During early grain filling, h_P was almost half of H_P but increased as the grains matured (Fig. 6a, b). Overall, H_P and h_P were significantly different between cultivars throughout the period ($p < 0.05$) (Fig. A1a, b). The high variation in H_P and h_P at the booting stage was mainly due to the samples from Senatore Capelli, a traditional and tall cultivar with H_P up to 1.1 m.

After both H_P (Fig. 6a) and fresh aerial biomass of the whole plant (FB_P) (Fig. 1) plateaued (Fig. 6c), h_P still increased (Fig. 6b) due to grain filling, i.e., the continued accumulation of dry biomass in the plant head. Large variation existed in the FB_P of different cultivars ($p < 0.001$), with cultivars such as Senatore Capelli, Odisseo and Marco Aurelio having relatively higher FB_P (Fig. A1c). The self-weight moment of the whole plant (M_P) was measured (using Eq.1) at six different crop angles of inclination (CAI) from the vertical - 10°, 20°, 30°, 40°, 45° and 60°. During our analysis we found that both M_P and S_A values increased linearly with increasing crop angle before levelling (slight decline) out at CAI of 30°, which was also consistent with the findings of Crook and Ennos (1994). The moment of decline is the maximum resistance and a good measure for root anchorage failure, after that moment the plants will lodge. Therefore, we selected the measurements made at CAI = 30° for subsequent analyses. M_P continued to rise after flowering, reaching its maximum at the milking stage (mean of 1.34 N-m) (Fig. 6d) when the plant ears were the heaviest (late May/beginning of June). The high M_P of Senatore Capelli, Odisseo and Marco Aurelio can be attributed to high h_P and FB_P (Fig. A1d).

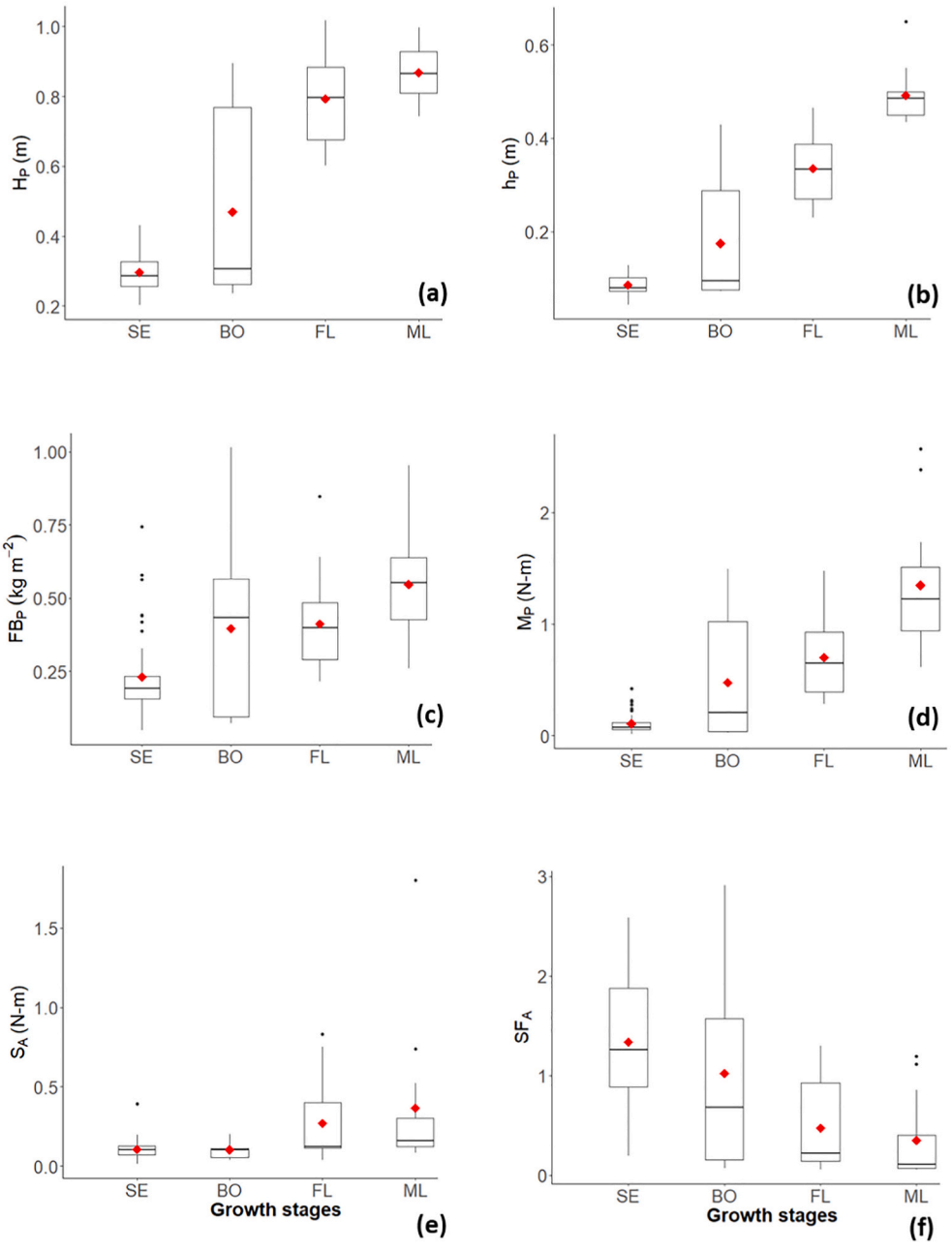

Fig. 6. Variation of measured crop biophysical parameters across the growing season. Boxplots illustrate plot-level variation in field-measured crop biophysical parameters: (a) plant height (H_P, m), (b) plant height at the center of gravity (h_P, m), (c) fresh aerial biomass (FB_P, kg m^{-2}), (d) self-weight moment of the whole plant at the crop angle of inclination of 30° (M_P, N-m), (e) anchorage strength at a crop angle of inclination of 30° (S_A, N-m) and (f) safety factor against root lodging at a crop angle of inclination of 30° (SF_A) across different growth stages ($n = 90$): stem elongation (SE), booting (BO), flowering (FL) and milking (ML). Boxplots display data distribution from bottom to top: lower whisker as a minimum, first quartile, median, third quartile and upper whisker as maximum. The black dots represent outliers, and red diamonds are mean values. (For interpretation of the references to colour in this figure legend, the reader is referred to the web version of this article.)

From the early stem elongation stage to crop maturation, mean root anchorage strength (S_A) increased from 0.11 to 0.36 N-m (Fig. 6e). In general, from the booting stage onwards, the mean S_A of the observed samples was lower than the mean M_P resulting in a mean crop safety factor against root lodging (SF_A) below 1 (Fig. 6e, Fig. A1e). There were minor differences in the M_P and S_A for different cultivars. For example, at the flowering stage, Massimo Meridio required the largest moment to push the plant over (mean $S_A = 0.45$ N-m) compared to other cultivars (mean $S_A = 0.20$ N-m) (Fig. A1e); still, Massimo Meridio's S_A was lower than its M_P. The maximum S_A of all cultivars over the entire observation period did not exceed 1 N-m, except for one Marco Aurelio sample (1.8 N-m at the milking stage) (Fig. A1e). The variation of SF_A across different growth stages is shown in Fig. 6f. The values of SF_A demonstrated a statistically significant decreasing trend as the crop matured ($p < 0.001$, Fig. 6f). SF_A was lowest during the flowering and grain filling phenological stages. The mean SF_A from the booting stage onwards was ≤ 1, which indicated that root lodging might have occurred from any point thereon.

3.2. Field-measured safety factor versus lodging susceptibility score of different cultivars

We further assessed the correlation between cultivar LSS and SF_A (Fig. 7). Based on the LSS, we categorized the cultivars as "low score" (<4.5) and "high score" (≥4.5); where the cultivars falling in the "high score" group were highly susceptible to lodging. A total of 44 out of 47 (i.e., 94%) samples were observed to be lodged in the study site and 30% of the samples falling in the "low score" group still lodged, showing that the cultivars with low LSS were, to some extent, still prone to lodging. This observation is not surprising because "cultivar susceptibility" is only one of the components of lodging risk that is strongly dependent on i) site-specific crop growth (i.e. seasonal susceptibility - SF_A) and ii) external driving forces (e.g. wind and rain).

3.3. Correlation analyses between remote sensing-based metrics and SF_A

Pearson correlation coefficients were used to quantify the relationship between RS-based metrics and SF_A and to identify the best performing metrics. Sentinel-1 has a shorter revisit time than RADARSAT-2 resulting in more images in the time-series. Therefore, 90 and 71 field samples were measured across the season for the analysis of Sentinel-1 and RADARSAT-2 data, respectively. Six out of nine Sentinel-1 metrics and 23 out of 39 RADARSAT-2 metrics had statistically significant correlations with SF_A (Fig. 8, Table A2, A3).

For Sentinel-1, the coherence in VV polarization ($\gamma_{VV}\gamma_{VV}$) showed the highest positive correlation with SF_A ($r = 0.64$) (Fig. 8a), suggesting that γ_{VV} provided the most reliable information for monitoring SF_A over the study area. Strong negative correlations were observed between SF_A and the $\sigma^o_{VH/VV}$, Anisotropy and Radar Vegetation Index (RVI) ($-0.57 < r < -0.60$) (Fig. 8a). High anisotropic scattering (>0.5) corresponded to low SF_A values (<1) while higher SF_A values (>1) exhibited low anisotropic scattering (<0.3).

For RADARSAT-2, the volume scattering component derived from Pauli decomposition (Pauli_vol) had the highest correlation with SF_A ($r = 0.71$) (Fig. 8b). The Span, biomass index and surface scattering component derived from Cloude decomposition (Cloude_surf) showed the same trend in correlation with SF_A ($r = 0.69$) (Fig. 8b). The correlation of SF_A with double-bounce scattering components derived from Pauli (Pauli_dbl, $r = 0.51$), Freeman-Durden (FD_dbl, $r = 0.37$) and Yamaguchi (Yama_dbl, $r = 0.24$) decomposition were statistically significant but lower than the other metrics (Table A3).

3.4. Estimation and mapping of the safety factor

XGB regression models were trained and validated using a five-fold Venetian blinds cross-validation. Fig. 9 displays the scatterplots between measured and predicted SF_A values, the cross-validated coefficient of determination (R^2_{CV}) and root mean square error ($RMSE_{CV}$) based on a regression analysis of SF_A against RS-based metrics. The predicted SF_A values were in strong agreement with the measured values when the backscattering coefficients, coherence, and polarimetric metrics (listed in Table A2) derived from Sentinel-1 were used as inputs, (R^2_{CV} $R^2_{CV} = 0.73$) (Fig. 9a). However, the results were penalized by some degree of underestimation for the high SF_A values (>2), resulting

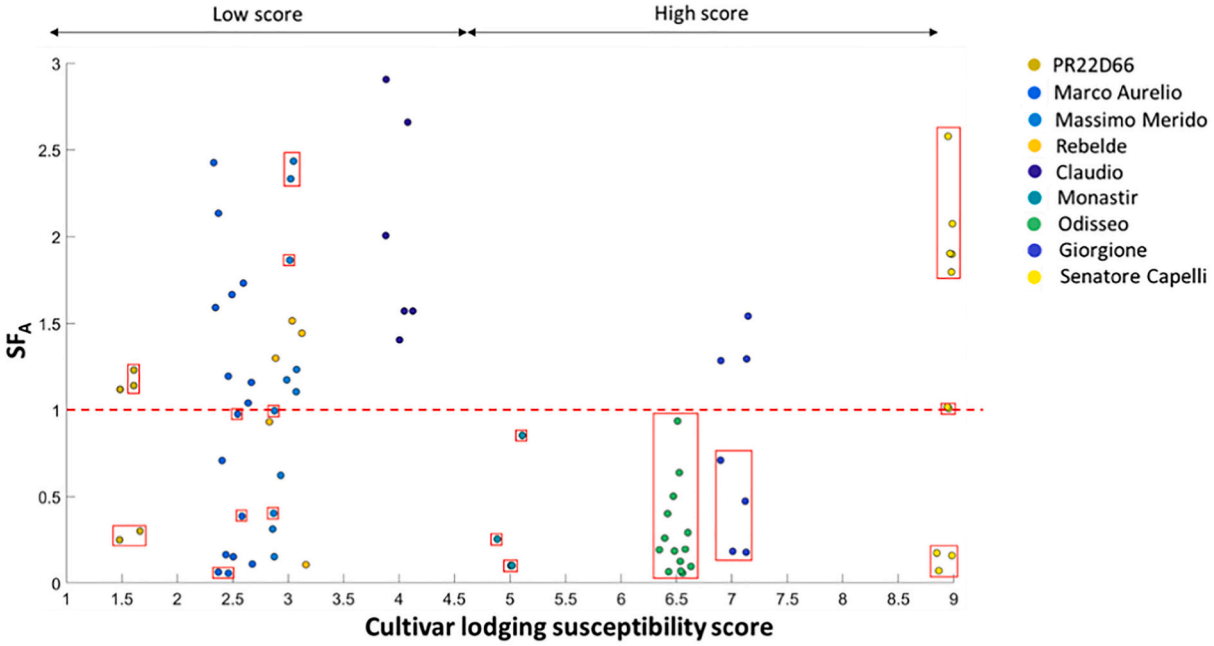

Fig. 7. Variation of the field-measured SF_A for different cultivar lodging susceptibility scores along the season ($n = 90$). Cultivars are categorized into low (<4.5) and high score (≥4.5) groups. The observed lodged samples are highlighted with red boxes. The dashed red line represents the critical threshold at $SF_A = 1$. Plots with $SF_A \leq 1$ signify that the crop is at high risk of being root lodged due to the self-weight moment while the ones with $SF_A > 1$ are at relatively lower root lodging risk. (For interpretation of the references to colour in this figure legend, the reader is referred to the web version of this article.)

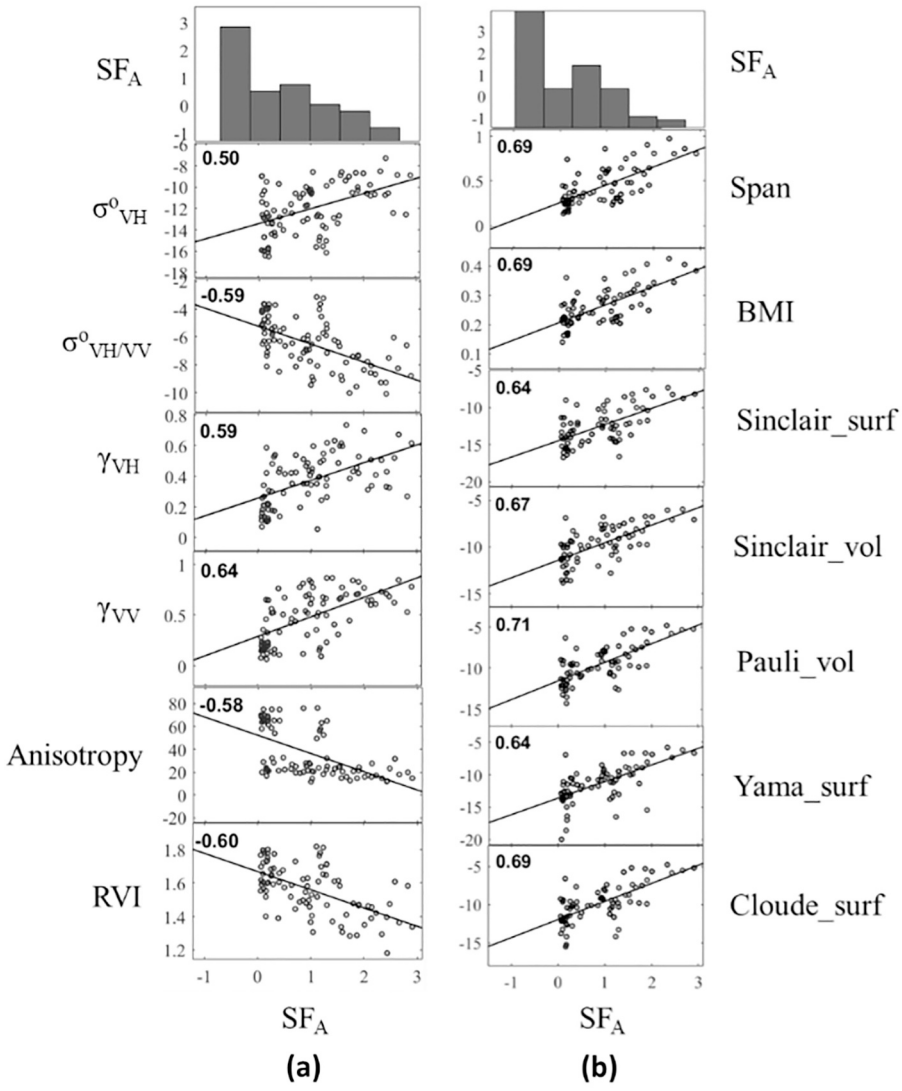

Fig. 8. Pearson correlation scatterplots of field measured SF_A against satellite metrics. Pearson correlation scatter plots of the most significant satellite metrics derived from (a) Sentinel-1 (n = 90), (b) RADARSAT-2 (n = 71) data and the field measured safety factor against root lodging (SF_A). The variation in the number of samples (n) for Sentinel-1 and RADARSAT-2 data is due to the difference in image availability between the two. All shown correlation coefficients between SF_A and satellite metrics are statistically significant at p = 0.01. σ^{o}_{VH} is the backscattering coefficient in VH polarization, $\sigma^{o}_{VH/VV}$ is the ratio of the backscattering coefficients in VH and VV polarizations, γ_{VH}, γ_{VV} are the interferometric coherences in VH and VV polarizations, RVI is the radar vegetation index, BMI is the biomass index, Sinclair_vol and Pauli_vol are the volume scattering components derived from Sinclair and Pauli decomposition respectively, and Yama_surf and Cloude_surf are the surface scattering components derived from Yamaguchi and Cloude decomposition respectively.

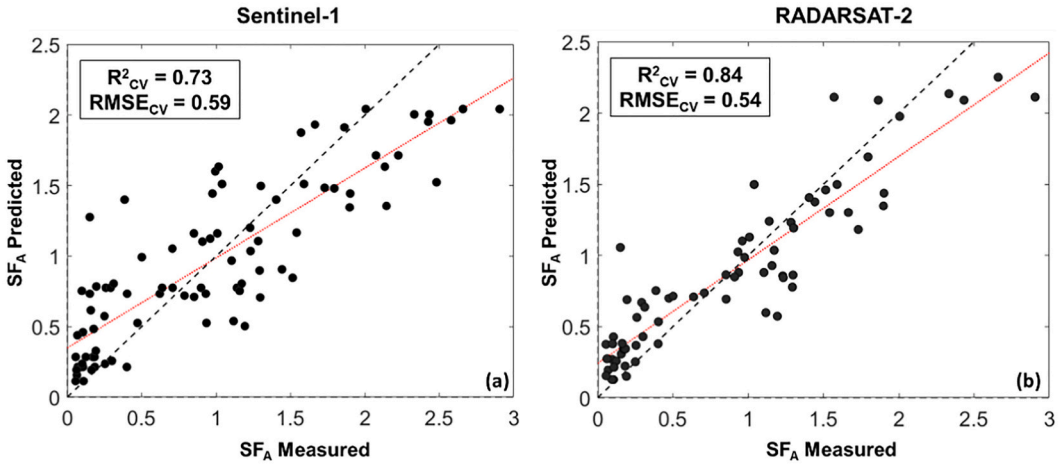

Fig. 9. Relationships between measured and predicted SF_A for Sentinel-1 and RADARSAT-2. Scatterplots show the relations between measured and predicted SF_A values obtained using cross-validated regression models for (a) Sentinel-1 (n = 90) and (b) RADARSAT-2 (n = 71) data. The variation in the number of samples (n) for Sentinel-1 and RADARSAT-2 data is due to the difference in the image availability for each sensor. The field data has been compiled for the entire season for different wheat cultivars. The black dashed line is the 1:1 line, while the red dotted line is the modeled regression line. The R^2_{CV} is the cross-validated coefficient of determination, and $RMSE_{CV}$ is the cross-validated root mean square error for each model. (For interpretation of the references to colour in this figure legend, the reader is referred to the web version of this article.)

in an $RMSE_{CV}$ of 0.59. This is evident from the dispersion of the samples around the 1:1 line in Fig. 9a. The degree of underestimation reduced when backscattering coefficients and polarimetric metrics derived from RADARSAT-2 were used, resulting in an $RMSE_{CV}$ of 0.54 (Fig. 9b). The predicted SF_A correlated strongly with the measured SF_A ($R^2_{CV} = 0.84$).

Cross validated XGB models were applied over the study site to map the spatial and temporal variability of SF_A. Fig. 10 illustrates the predicted SF_A maps derived from Sentinel-1 (March 26) and RADARSAT-2 (April 2) datasets over the wheat fields. These dates were selected to demonstrate the potential of indicating root lodging susceptibility early in the season (early spring) when the crop is in the stem elongation growth stage. The underestimation of high SF_A values is apparent in the Sentinel-1 map (Fig. 10a). However, the spatial distribution of predicted SF_A in both maps shows that areas where SF_A is 1 (or less), it is likely that the gravitational forces due to M_P of the whole plant alone could cause lodging. The areas with $SF_A > 1$ indicate that M_P alone may not cause lodging.

4. Discussion

4.1. Safety factor prediction using Sentinel-1 and RADARSAT-2 data

Microwave scattering is mainly governed by crop macrostructure (such as plant density or row spacing), plant dielectric properties and canopy structure (shape, size and orientation of plant constituents) (Wang et al., 2019). C-band SAR, to a certain degree, can penetrate the crop canopy, which also results in a contribution from the soil in the total backscatter signal (soil roughness and moisture). This is especially true in the early growth stages when the crop cover is less dense. Polarimetric decomposition parameters can be used to separate the vegetation contributions from the total backscatter. The better performance of the RADARSAT-2 (quad-polarization mode with HH, HV, VH and VV channels) model can be attributed to a rich set of polarimetric decomposition metrics. Sentinel-1 has a higher revisit time, but its data is available only in the dual-polarization mode, which restricts the usage to just one cross-polar (VH) and one copolar channel (VV). This results in fewer metrics and lower SF_A retrieval accuracy. However, the synergic use of backscattering coefficients and interferometric coherence in Sentinel-1 enhanced the estimation of SF_A ($R^2_{CV} = 0.73$, $RMSE_{CV} = 0.59$), over using backscattering coefficients alone.

Even though the scattering from crop and attenuation effects are complexly coupled in wheat (Ferrazzoli, 2002; Wang et al., 2019), the XGB models were able to capture the coupling pattern, resulting in a robust SF_A retrieval ($R^2_{CV} > 0.70$; $RMSE_{CV} < 0.60$) (Fig. 9). However, there are two issues that should be mentioned here. Firstly, the underestimation of both models at high SF_A values (>2) can perhaps be explained by the saturation of the backscatter and polarimetric parameters with high plant height and fresh aerial biomass values due to pronounced scattering from wheat heads (Bouman and van Kasteren, 1989; Harfenmeister et al., 2019; Yan et al., 2019). Moreover, the general tendency of the regression models to underestimate large magnitudes cannot be neglected. This phenomenon has been reported in diverse experimental settings and is likely to represent a general response bias under uncertainty (Karolis et al., 2011). Despite this, the critical SF_A value (close to 1) required to assess root lodging susceptibility in wheat could be detected by both Sentinel-1 and RADRSAT-2-based models (Fig. 9). Hence, the identified underestimation is not considered critical for highlighting spatially explicit zones of potential lodging susceptibility that can occur later in the crop season. The predicted SF_A maps demonstrate the capability of SAR data for geospatial mapping SF_A in wheat and can consequently be used as an indicator of root lodging susceptibility early in the season. Secondly, it is possible that the relationship between SF_A and SAR parameters is confounded by variations in crop biophysical parameters such as biomass, which is highly correlated to SF_A ($r = -0.71$, $p < 0.0001$). The correlation of such parameters with SF_A may also largely reflect in the sensitivity of the radar measurements to SF_A. The accuracy may further be improved by reducing the effects of such confounding factors through sample stratification (not shown). However, this is out of the current manuscript's scope but can be addressed in further work.

4.2. Relationship between satellite metrics and SF_A

The correlation analyses between the RS-based metrics and field measured SF_A identified the most significant parameters for estimating SF_A from satellite data. In general, the r values were higher for RADARSAT-2 derived metrics (Fig. 8b). The microwave signal is highly sensitive to the structure and geometry of the canopy and is a function of size, orientation and density of the scatterers/target (Chauhan et al., 2018). As a microwave signal hits the crop canopy, there are three forms of scattering mechanisms that can occur: surface/single-bounce, double-bounce, and volume scattering. The higher relative correlation of the volume scattering components such as Pauli_vol ($r = 0.71$) and Sinclair_vol ($r = 0.67$) (Fig. 8b) with SF_A possibly indicates the dominance of the volume scattering mechanism as the crop grows. The decrease in SF_A across different growth stages (Fig. 6f) indicates the increasing

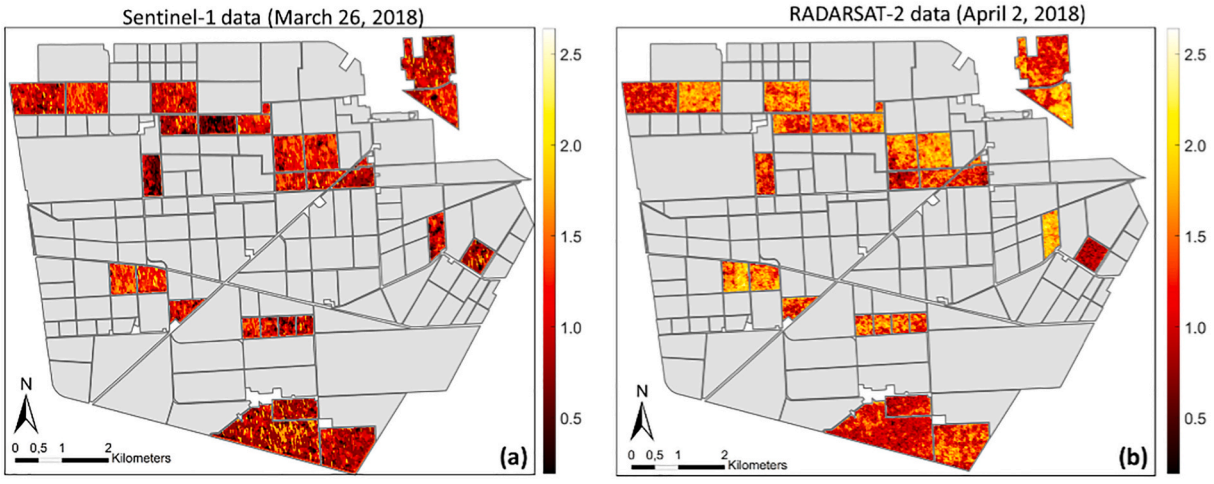

Fig. 10. Spatial distribution of SF_A in the study area. SF_A in wheat fields in study site obtained from the cross-validated regression models using inputs from (a) Sentinel-1 (image on March 26, 2018) and (b) RADARSAT-2 (image on April 2, 2018). Wheat was in the stem elongation growth stage. The farm boundaries are also overlaid on the maps. Non-wheat fields are gray. "RADARSAT-2 Data and Products. MacDonald, Dettwiler and Associates Ltd. (2018) – All Rights Reserved. RADARSAT is an official trademark of the Canadian Space Agency."

susceptibility of root lodging during the season as the M_P exceeded S_A in our study site. However, we would like to emphasize that the average decreasing trend of SF_A (Fig. 6f) over the season is not always the case (as observed for most of the cases in our study site). If the root structure is strong enough to compensate for the increased M_P, the safety factor may show an increasing trend (Crook and Ennos, 1994). The decrease in SF_A with the crop growth in our case is because the rate of increase in M_P is much higher than the increase in S_A (Fig. 6d, e). And since the increase in M_P (which is composed of biomass, crop height and crop angle of inclination) is the main factor here governing the SF_A trend, the volumetric component is increasing due to increasing crop volume.

It should also be emphasized here that the contribution of azimuth slope and soil roughness on elevated cross-polarized response can be considered negligible here since (i) we applied orientation angle correction to remove the orientation angle shift caused by azimuth slopes from the polarimetric SAR data, (ii) unlike lower frequencies (such as L-band), higher frequency PolSAR responses (such as from C-band) are less sensitive to azimuth slope variations, because electromagnetic waves with shorter wavelengths are less penetrative and more sensitive to small scatterers (Lee and Pottier, 2017) and lastly (iii) wheat fields had similar soil roughness, approximately 1 cm in average, with minimal changes during the entire crop development.

We also found evidence of a certain degree of surface scattering from the wheat fields, which is depicted by a moderate correlation between SF_A and the Cloude_surf metric ($r = 0.69$) (Fig. 8b). The presence of surface scattering confirms some degree of backscatter contribution from the soil attenuated by vegetation canopy. Typically, either of the scattering mechanisms dominates, however for distributed targets (such as an agricultural field), secondary or tertiary scattering mechanisms can also occur (Steele-Dunne et al., 2017). At the beginning of the season when the crop cover is less dense, surface scattering dominates (soil is the dominant contributing factor) and with the development of crop canopy volume scattering becomes more dominant, although the surface scattering is still evident, due to a quite probable horizontal orientation resulting from the bending of leaves (Chauhan et al., 2018). Furthermore, SF_A is a parameter that is sensitive to both crop (M_P) and soil components (S_A). Therefore, our analyses showed that a mixture of volume and surface scattering types characterized the crop canopy. Similar observations were also made by Kar et al. (2017).

For Sentinel-1 data, the interferometric coherence in the VV polarization showed the highest positive correlation with SF_A ($r = 0.64$) (Fig. 8a). Interferometric coherence at any polarization is not only sensitive to the dielectric properties, orientation and shape of plant constituents but also the vertical structure of the plant (Lopez-Sanchez and Ballester-Berman, 2009). Studies have shown that a strong linear relationship exists between plant height and coherence (Khabbazan et al., 2019; Vreugdenhil et al., 2018). At the same time, at VV polarization, the contribution from the upper canopy dominates for incidence angles $>37^o$, due to the presence of flag leaves and ears (Brown et al., 2003). With the increasing plant height (Fig. 6a) and fresh biomass (Fig. 6c), the SF_A decreases (Fig. 6f). As plant height is inversely proportionate to the interferometric coherence (Engdahl et al., 2001), a positive correlation emerged between SF_A and VV coherence values. We should also emphasize here that based on the insights gained from previous studies (Ghosh et al., 2020; Khabbazan et al., 2019; Shang et al., 2020), we assumed that the changes in vegetation structure (increase in plant height and reduction in SF_A along the crop growth) resulted in temporal decorrelation and therefore, the change in coherence. The negative correlation of SF_A with RVI and $\sigma^o_{VH/VV}$ (Fig. 8a) could be attributed to the increase in RVI and $\sigma^o_{VH/VV}$ from booting to flowering as the plant biomass accumulates. The increasing RVI and $\sigma^o_{VH/VV}$ at the beginning of the vegetation period indicate the attenuation of the radar signal by growing vegetation. Similar results have also been reported by Mandal et al. (2020) for wheat crop during these growth stages. Furthermore, a high anisotropic scattering (>0.5) for low SF_A values (<1) indicates two dominant scattering mechanisms with almost equal probability and a less significant third scattering mechanism. Lower anisotropic scattering (<0.3) for higher SF_A values (>1), on the other hand, shows that there is only one dominant scattering mechanism with two non-negligible secondary mechanisms with equal importance. However, it is difficult to point out which scattering mechanism is dominant and which is not solely based on dual-polarimetric Sentinel-1data. The polarimetric parameters derived from RADARSAT-2 quad-pol data complemented these observations (as shown above).

Furthermore, there are studies that explain the effect of soil moisture, roughness and texture on SAR backscatter (Balenzano et al., 2010; Srivastava et al., 2003), there is limited knowledge on the how SAR data is responsive to soil structural properties such as soil shear strength and root plate diameter (factors that govern root anchorage strength). An analysis in this regard is beyond the scope of this study and should be researched in future studies. A study done by Rabus et al. (2010) does shed some light on how backscatter and interferometric phase information can infer near soil structural parameters such as vertical gradients and inhomogeneities, the research is in a very nascent stage and was performed in simulated conditions. However, the results are promising and must be explored further to study other soil structural traits (such as root anchorage strength).

Overall, although both Sentinel-1 and RADARSAT-2 sensors operate at the same frequency C-band, differences in other sensor characteristics such as polarization (dual and quad-pol), incidence angle (40° and 27°-41°), radiometric accuracy (1 dB and < 1 dB) and spatial resolution (15× 15 m and 10 × 10 m) resulted in varying performances of the two sensors. The *r* values for RVI (radar vegetation index) (Table A2, A3) are particularly different for Sentinel-1 and RADARSAT-2. This could be attributed to different polarization channels that are used in the formulation of RVI for Sentinel-1 ($RVI = 4\ \sigma^o_{VH}/(\sigma^o_{VH} + \sigma^o_{VV})$) and RADARSAT-2 ($RVI = 8\ \sigma^o_{HV}/(\sigma^o_{HH} + \sigma^o_{VV} + 2\ \sigma^o_{HV})$).

4.3. Variability in the field measured crop biophysical parameters

Plant height (H_P) and height at the center of gravity (h_P) are important factors influencing lodging susceptibility in wheat (Berry et al., 2000). h_P is influenced by both H_P and ear biomass (Berry et al., 2000). With grain filling, ear biomass increases, and straw biomass reduces, thus raising h_P. The self-weight moment of the whole plant (M_P), which approximates the wind-induced base bending moment that a plant experiences, increased as the crop matured (Fig. 6d). This could be due to the increase in both h_P and FB_P.

Root system architecture plays an essential role in anchoring the plant to soil. It has been demonstrated that S_A is a function of mechanical properties such as root plate diameter and soil shear strength (van Delden et al., 2010) (Fig. 1). S_A increased as the crop matured, which is possibly due to the increase in the depth and spread of the root plate diameter (Berry et al., 2000) The susceptibility of root lodging increases if M_P exceeds S_A (Crook and Ennos, 1993) and can be quantified using SF_A (Eq. 2). In most cases, S_A was less than M_P (Fig. 6d, e). A relatively high S_A (1.8 N-m) for one of Marco Aurelio samples can be explained by the low seed rate in this plot, which might have increased the S_A by increasing the root plate spread (Berry et al., 2000). The decrease in SF_A across different growth stages (Fig. 6f) indicated the increasing susceptibility of root lodging during the season due to the plant self-weight moment alone as M_P exceeded S_A. Lower S_A resulted in a lower SF_A later in the season, implying that root-soil anchorage may not be able to resist the overturning moments produced by the plant's self-weight, even though only gravitational forces were considered. Therefore S_A should be improved to increase root lodging resistance (Wu et al., 2019). A rigid root system can be developed by enabling enlarged root spread through low seed rate, increasing soil shear strength and stimulating greater proportion of assimilates to be partitioned into the roots (Li et al., 2018; Wu et al., 2012). SF_A does not account for the forces generated by wind, which can further intensify the overturning moments and can

progressively weaken the root-soil anchorage (Coutts, 1983).

4.4. Field measured safety factor versus observed lodging

The observed rate of lodging was high throughout the growing season, with most cases coinciding with grain filling when the ears were heaviest. Root lodging was the primary cause of failure (80% of cases). The measured SF_A was largely consistent with field recorded observations of lodging (Fig. 11a). The time when SF_A dropped to the absolute critical value of 1, coincided with the observed onset of lodging in the field (i.e., at the end of the booting stage) (Fig. 6f); 33 samples were non-lodged while 57 samples had lodged with different degrees of severity. Furthermore, as shown in Fig. 11a, 24 out of 33 healthy samples corresponded to $SF_A > 1$, i.e., 73% of the samples were correctly identified as having no root lodging susceptibility using the SF_A while 42 out of 57 lodged samples corresponded to $SF_A \leq 1$, meaning that 74% of the samples were correctly identified as susceptible to root lodging using the SF_A. A direct comparison of the remotely sensed SF_A (predicted using Sentinel-1 and RADARSAT-2) and actual lodging is also shown in Fig. 11b. Almost 60% and 77% of the lodged samples were correctly predicted to have the $SF_A \leq 1$ using Sentinel-1 and RADARSAT-2 data respectively. A comparison within and across different wheat cultivars at specific growth stages is also presented in the appendix (Table A4) demonstrating how the root lodging susceptibility (high/low) predicted using SF_A correlate with the actual crop condition (lodged/non-lodged) observed on the field around the harvest time. Based on the analysis, we can say that the SF_A assessment resulted in an overall agreement with the observed lodging phenomena.

Currently, LSS serves as the only measure for farmers to indicate the theoretical relative lodging susceptibility for each cultivar. However, LSS does not explain the reason for a high or low susceptibility of a cultivar. The relative strength of the stem base and the roots as depicted by M_P and S_A (see Fig. A1d, e) can explain the variation in LSS for each cultivar. For instance, the high LSS (6.5) of the cultivar Odisseo is probably explained by very low root anchorage strength (S_A) and safety factor (SF_A), resulting from poor root structure (Fig. A1). Similarly, a very low self-weight moment (M_P) for the cultivar Senatore Capelli, indicates that poor stem structure might explain a high LSS (9) (Fig. A1). This information can be beneficial as it gives a better idea to the farmers about which section of the plant to target for lodging control. In this context, for a cultivar such as Odisseo, it might be more important to take measures to boost the soil/root structure (e.g. through lower seed rate or rolling), while for Senatore Capelli with weaker stem structure, using plant growth regulators can be useful. For cultivars with a good root and stem structure (such as Monastir), careful management along with low plant growth regulator input could be sufficient to reduce lodging susceptibility. Thus, an understanding in the variation of SF_A (and its components), in addition to a cultivar LSS, can result in informed cultivar choice.

4.5. Recommendations and perspectives

The primary advantage of using a safety factor against root lodging (SF_A) as an indicator of crop lodging susceptibility is that it is simple, allows quantitative analysis of the variation in root lodging resistance and, above all, is detectable over large areas using operational remote sensing platforms. The RS model can be applied to other locations under similar conditions, but this will require model validation using a small number of SF_A field measurements. The SF_A measure thus constitutes a state-of-the-art approach for the assessment of root lodging susceptibility early in the season. Information about SF_A can be used to develop optimum crop management practices in almost real-time, for instance, adjusting the use of plant growth regulators later in the season, as the maps can be generated early in the spring when the crop completes the stem elongation period. The use of SF_A as an indicator to guide nitrogen fertilizer applications and mitigate lodging susceptibility would further validate the effectiveness of the SF_A method.

SF_A does not directly account for wind or rain-induced forces; neither does SF_A explicitly consider the environmental or other management-related parameters, SF_A is simply a measure of lodging susceptibility. This study provides a basis for future research efforts that could benefit from the incorporation of the SF_A parameter in lodging risk assessments. For example, SF_A could be combined with long term climate averages (for baseline risks), forecasts of precipitation and wind gusts, soil properties and other remotely sensed crops biophysical and biochemical parameters (such as plant area index and plant nitrogen) to provide more accurate and timely risk assessments. Also, despite the diverse dataset used in this work, the robustness and reproducibility must be assessed further in other environmental, soil and management conditions for wheat as well as other crops using a multi-season and more contrasted dataset. Although stem lodging was almost neglectable for the cultivars in our study area (only 15 plots showed an occurrence of stem lodging contrary to 30 plots with root lodging), an RS-based investigation of the safety factors against stem lodging is another potential topic of research. Regardless of the assumptions behind the formulation of SF_A, our study demonstrates that time-series of RS data can be used effectively to estimate root lodging susceptibility at the field scale and offers a preview of further opportunities in making lodging risk analysis more robust and accurate.

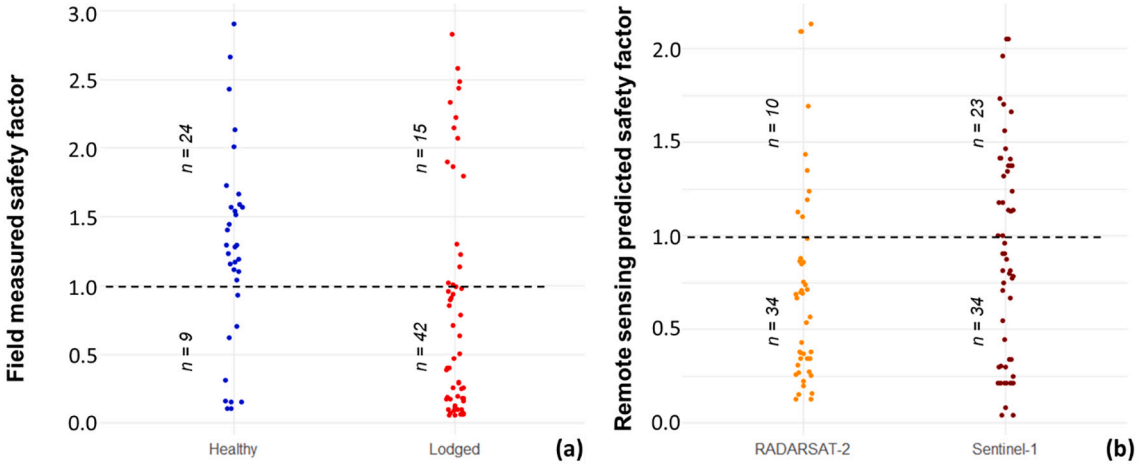

Fig. 11. Dot plot showing the distribution of (a) field measured SF_A for healthy ($n = 33$) and lodged ($n = 57$) samples and (b) actual lodged samples against Sentinel-1 ($n = 57$) and RADARSAT-2 ($n = 44$) derived SF_A. The black dotted line indicates the safety factor lodging threshold (i.e., $SF_A = 1$) considered in this study.

5. Conclusions

This study aims to quantify the utility of fine spatial resolution SAR imagery as acquired from commercial and open-access satellite platforms for the estimation of SF_A in wheat crop. First, we analyzed and interpreted the temporal trend of the field measurements across different growth stages. A suite of RS-based metrics was also correlated with the field measured SF_A for different plots to understand the strength of correlation and enable interpretation of the regression models. Lastly, we developed two XGB regression models using the inputs from Sentinel-1 and RADARSAT-2 data to estimate SF_A and map its spatial distribution across the study site. We also validated field measured SF_A with the occurrence of lodging in the field. The key conclusions are summarized below:

a) The SF_A showed a decreasing trend as the crop matured, with the lowest values during the flowering and grain filling period when the lodging risk is the highest.
b) In general, most of the RS-based metrics showed a statistically significant correlation with SF_A values, particularly the biomass index, VV coherence, span, Pauli volume scattering component and Cloude surface scattering components ($r > 0.60$).
c) The cross-validated XGB model using the inputs from RADARSAT-2 data ($R^2_{CV} = 0.84$, $RMSE_{CV} = 0.54$) outperformed the Sentinel-1 model ($R^2_{CV} = 0.73$, $RMSE_{CV} = 0.59$), with some degree of underestimation at high SF_A (>2) values. The resulting maps also successfully captured the spatial variation in SF_A. However, estimation of SF_A with SAR data might be confounded by variations in crop biomass, (correlation of $r = -0.71$, $p < 0.0001$) and the estimation accuracy of SF_A can further be improved by reducing the effects of such confounding factors through sample stratification in future work.
d) The field measured SF_A correlated well with the lodging observed on the field. The time when SF_A reached the critical threshold of 1, coincided with the time when the first few instances of lodging were observed in the field (i.e. during the booting stage). 70% of the actual healthy samples corresponded to $SF_A > 1$ while 74% of the lodged samples had $SF_A \leq 1$, which indicates the utility of RS-derived SF_A as an early measure of root lodging risk.

The SF_A measure constitutes a state-of-the-art approach in the RS community for the assessment of root lodging susceptibility early in the season. However, we emphasize that SF_A does not account for the external wind or rain-induced forces and neither the environmental and other management-related parameters are considered in this study. These parameters when incorporated in a model can provide more robust lodging risk estimates. This study provides a basis for future research efforts which could benefit from the incorporation of SF_A parameter along with other lodging sensitive parameters in a lodging risk model. The investigation of the assessment of RS-based stem lodging susceptibility using safety factors against stem lodging is another potential topic of research. Nevertheless, this study demonstrates that the time-series RS data from different sources can be used effectively for detecting root lodging susceptibility at the field scale.

Declaration of Competing Interest

The authors declare that they have no known competing financial interests or personal relationships that could have appeared to influence the work reported in this paper.

Acknowledgements

The authors thank the University of Twente for funding the research and all those who actively participated in the field campaign in 2018. We are grateful to Dr. Donato Cillis of IBF–S technical team for his support and the Bonifiche Ferraresi farm for hosting the experimentation and for supporting the field activities for the period 2017–2018. The authors also thank MDA-GSI and the Canadian Government for providing RADARSAT-2 data through the project "Vegetation parameter retrieval from SAR data", number SOAR-EI-5446.

Appendix A. Supplementary data

Supplementary data to this article can be found online at https://doi.org/10.1016/j.rse.2021.112427.

References

Allison, G.G., Morris, C., Hodgson, E., Jones, J., Kubacki, M., Barraclough, T., Yates, N., Shield, I., Bridgwater, A.V., Donnison, I.S., 2009. Measurement of key compositional parameters in two species of energy grass by Fourier transform infrared spectroscopy. Bioresour. Technol. 100, 6428–6433.
Balenzano, A., Mattia, F., Satalino, G., Davidson, M.W.J., 2010. Dense temporal series of C-and L-band SAR data for soil moisture retrieval over agricultural crops. IEEE J. Sel. Top. Appl. Earth Obs. Remote Sens. 4, 439–450.
Berry, P.M., Spink, J.H., 2012. Predicting yield losses caused by lodging in wheat. F. Crop. Res. 137, 19–26.
Berry, P.M., Griffin, J.M., Sylvester-Bradley, R., Scott, R.K., Spink, J.H., Baker, C.J., Clare, R.W., 2000. Controlling plant form through husbandry to minimise lodging in wheat. F. Crop. Res. 67, 59–81.
Berry, P.M., Spink, J.H., Gay, A.P., Craigon, J., 2003a. A comparison of root and stem lodging risks among winter wheat cultivars. J. Agric. Sci. 141, 191–202.
Berry, P.M., Sterling, M., Baker, C.J., Spink, J.H., Sparkes, D.L., 2003b. A calibrated model of wheat lodging compared with field measurements. Agric. For. Meteorol. 119, 167–180.
Berry, P.M., Sterling, M., Spink, J.H., Baker, C.J., Sylvester-Bradley, R., Mooney, S.J., Tams, A.R., Ennos, A.R., 2004. Understanding and reducing lodging in cereals. Adv. Agron. 84, 215–269.
Bleiholder, H., Weber, E., Lancashire, P.D., Feller, C., Buhr, L., Hess, M., Wicke, H., Hack, H., Meier, U., Klose, R., 2001. Growth Stages of Mono-and Dicotyledonous Plants, BBCH Monograph. Federal Biological Research Centre for Agriculture and Forestry, Berlin/Braunschweig, Germany.
Bock, C.H., Poole, G.H., Parker, P.E., Gottwald, T.R., 2010. Plant disease severity estimated visually, by digital photography and image analysis, and by hyperspectral imaging. CRC. Crit. Rev. Plant Sci. 29, 59–107.
Bouman, B.A.M., van Kasteren, H.W.J., 1989. Ground Based X-Band Radar Backscatter Measurements of Wheat. Barley and Oats, pp. 1975–1981.
Brown, S.C.M., Quegan, S., Morrison, K., Bennett, J.C., Cookmartin, G., 2003. High-resolution measurements of scattering in wheat canopies-implications for crop parameter retrieval. IEEE Trans. Geosci. Remote Sens. 41, 1602–1610.
Caldicott, J.J.B., Nuttall, A.M., 1979. A method for the assessment of lodging in cereal crops. J. Natl. Inst. Agric. Bot. 15, 88–91.
Charbonneau, F., Trudel, M., Fernandes, R., 2005. Use of Dual Polarization and Multi-Incidence SAR for soil permeability mapping. In: Adv. Synth. Aperture Radar St-Hubert, QC, Canada.
Chauhan, S., Srivastava, H.S., Patel, P., 2018. Wheat crop biophysical parameters retrieval using hybrid-polarized RISAT-1 SAR data. Remote Sens. Environ. 216, 28–43.
Chauhan, S., Darvishzadeh, R., Boschetti, M., Nelson, A., 2020a. Discriminant analysis for lodging severity classification in wheat using RADARSAT-2 and Sentinel-1 data. ISPRS J. Photogramm. Remote Sens. 164, 138–151.
Chauhan, S., Darvishzadeh, R., Boschetti, M., Nelson, A., 2020b. Estimation of crop angle of inclination for lodged wheat using multi-sensor SAR data. Remote Sens. Environ. 236, 111488.
Chauhan, S., Darvishzadeh, R., Lu, Y., Boschetti, M., Nelson, A., 2020c. Understanding wheat lodging using multi-temporal Sentinel-1 and Sentinel-2 data. Remote Sens. Environ. 243, 111804.
Chen, T., Guestrin, C., 2016. XGBoost: a scalable tree boosting system. In: Proc. ACM SIGKDD Int. Conf. Knowl. Discov. Data Min. 13-17-Augu, pp. 785–794.
Chen, J., Li, H., Han, Y., 2016. Potential of RADARSAT-2 data on identifying sugarcane lodging caused by typhoon. In: 5th Int. Conf. Agro-Geoinformatics, Agro-Geoinformatics, pp. 1–6.
Cloude, S.R., Pottier, E., 1996. A review of target decomposition theorems in radar polarimetry. IEEE Trans. Geosci. Remote Sens. 34, 498–518.
Coutts, M.P., 1983. Development of the structural root system of Sitka spruce. For. An Int. J. For. Res. 56, 1–16.
Crook, M.J., Ennos, A.R., 1993. The mechanics of root lodging in winter wheat, Triticum Aestivum L. J. Exp. Bot. 44, 1219–1224.
Crook, M.J., Ennos, A.R., 1994. Stem and root characteristics associated with lodging resistance in four winter wheat cultivars. J. Agric. Sci. 123, 167.
Crook, M.J., Ennos, A.R., 1995. The effect of nitrogen and growth-regulators on stem and root characteristics associated with lodging in 2 cultivars of winter-wheat. J. Exp. Bot. 46, 931–938.
Crook, M.J., Ennos, A.R., 2000. A field based method of quantifying the lodging resistance of wheat cultivars. Plant Biomech 315–320.
Darvishi, M., Schlögel, R., Kofler, C., Cuozzo, G., Rutzinger, M., Zieher, T., Toschi, I., Remondino, F., Mejia-Aguilar, A., Thiebes, B., others, 2018. Sentinel-1 and ground-

based sensors for continuous monitoring of the Corvara landslide (South Tyrol, Italy). Remote Sens. 10, 1781.
Engdahl, M.E., Borgeaud, M., Rast, M., 2001. The use of ERS-1/2 tandem interferometric coherence in the estimation of agricultural crop heights. IEEE Trans. Geosci. Remote Sens. 39, 1799–1806.
Ferrazzoli, P., 2002. SAR for agriculture: Advances, problems and prospects. In: Retrieval of Bio-and Geo-Physical Parameters from SAR Data for Land Applications, pp. 47–56.
Fischer, R.A., Stapper, M., 1987. Lodging effects on high-yielding crops of irrigated semidwarf wheat. F. Crop. Res. 17, 245–258.
Ghosh, S.M., Behera, M.D., Paramanik, S., 2020. Canopy height estimation using sentinel series images through machine learning models in a mangrove Forest. Remote Sens. 12, 1519.
Harfenmeister, K., Spengler, D., Weltzien, C., 2019. Analyzing temporal and spatial characteristics of crop parameters using Sentinel-1 backscatter data. Remote Sens. 11, 1569.
Kar, S., Mandal, D., Bhattacharya, A., Adinarayana, J., 2017. Temporal analysis of Touzi parameters for wheat crop characterization using L-band AgriSAR 2006 data. In: 2017 IEEE International Geoscience and Remote Sensing Symposium (IGARSS), pp. 3909–3912.
Karolis, V., Iuculano, T., Butterworth, B., 2011. Mapping numerical magnitudes along the right lines: differentiating between scale and bias. J. Exp. Psychol. Gen. 140, 693.
Khabbazan, S., Vermunt, P., Steele-Dunne, S., Ratering Arntz, L., Marinetti, C., van der Valk, D., Iannini, L., Molijn, R., Westerdijk, K., van der Sande, C., 2019. Crop monitoring using Sentinel-1 data: a case study from the Netherlands. Remote Sens. 11, 1887.
Lee, J.S., Pottier, E., 2017. Polarimetric Radar Imaging: From Basics to Applications. CRC press.
Li, P.F., Ma, B.L., Xiong, Y.C., 2018. Modern hexaploid wheat differs from diploid and tetraploid ancestors in the importance of stress tolerance versus stress avoidance. Crop Pasture Sci. 69, 265–277.
Lopez-Sanchez, J.M., Ballester-Berman, J.D., 2009. Potentials of polarimetric SAR interferometry for agriculture monitoring. Radio Sci. 44, 1–20.
Mandal, D., Kumar, V., Ratha, D., Dey, S., Bhattacharya, A., Lopez-Sanchez, J.M., McNairn, H., Rao, Y.S., 2020. Dual polarimetric radar vegetation index for crop growth monitoring using sentinel-1 SAR data. Remote Sens. Environ. 247, 111954.
Nelson, A., Setiyono, T., Rala, A.B., Quicho, E.D., Raviz, J.V., Abonete, P.J., Maunahan, A.A., Garcia, C.A., Bhatti, H.M., Villano, L.S., Thongbai, P., Holecz, F., Barbieri, M., Collivignarelli, F., Gatti, L., Quilang, E.J.P., Mabalay, M.R.O., Mabalot, P.E., Barroga, M.I., Bacong, A.P., Detoito, N.T., Berja, G.B., Varquez, F., Wahyunto, Kuntjoro, D., Murdiyati, S.R., Pazhanivelan, S., Kannan, P., Nirmala Mary, P.C., Subramanian, E., Rakwatin, P., Intrman, A., Setapayak, T., Lertna, S., Minh, V.Q., Tuan, V.Q., Duong, T.H., Quyen, N.H., Van Kham, D., Hin, S., Veasna, T., Yadav, M., Chin, C., Ninh, N.H., 2014. Towards an operational SAR-based rice monitoring system in Asia: examples from 13 demonstration sites across Asia in the RIICE project. Remote Sens. 6, 10773–10812.
Pinthus, M.J., 1974. Lodging in wheat, barley, and oats: the phenomenon, its causes, and preventive measures. Adv. Agron. 25, 209–263.
Rabus, B., Wehn, H., Nolan, M., 2010. The importance of soil moisture and soil structure for InSAR phase and backscatter, as determined by FDTD modeling. IEEE Trans. Geosci. Remote Sens. 48, 2421–2429.
Shang, J., Liu, J., Poncos, V., Geng, X., Qian, B., Chen, Q., Dong, T., Macdonald, D., Martin, T., Kovacs, J., others, 2020. Detection of crop seeding and harvest through analysis of time-series Sentinel-1 interferometric SAR data. Remote Sens. 12, 1551.
Souissi, B., Ouarzeddine, M., 2016. Analysis of orientation angle shifts on the polarimetric data using RadarSAT2 images. IEEE J. Sel. Top. Appl. Earth Obs. Remote Sens. 9, 1331–1342.
Srivastava, H.S., Patel, P., Manchanda, M.L., Adiga, S., 2003. Use of multiincidence angle RADARSAT-1 SAR data to incorporate the effect of surface roughness in soil moisture estimation. IEEE Trans. Geosci. Remote Sens. 41, 1638–1640.
Steele-Dunne, S.C., McNairn, H., Monsivais-Huertero, A., Judge, J., Liu, P.W., Papathanassiou, K., 2017. Radar remote sensing of agricultural canopies: a review. IEEE J. Sel. Top. Appl. Earth Obs. Remote Sens. 10, 2249–2273.
Torres-Barrán, A., Alonso, Á., Dorronsoro, J.R., 2019. Regression tree ensembles for wind energy and solar radiation prediction. Neurocomputing 326, 151–160.
Touzi, R., Lopes, A., Bruniquel, J., Vachon, P.W., 1999. Coherence estimation for SAR imagery. IEEE Trans. Geosci. Remote Sens. 37, 135–149.
van Delden, S.H., Vos, J., Ennos, A.R., Stomph, T.J., 2010. Analysing lodging of the panicle bearing cereal teff (Eragrostis tef). New Phytol. 186, 696–707.
Vreugdenhil, M., Wagner, W., Bauer-Marschallinger, B., Pfeil, I., Teubner, I., Rüdiger, C., Strauss, P., 2018. Sensitivity of Sentinel-1 backscatter to vegetation dynamics: an Austrian case study. Remote Sens. 10, 1396.
Wang, H., Magagi, R., Goïta, K., Trudel, M., McNairn, H., Powers, J., 2019. Crop phenology retrieval via polarimetric SAR decomposition and random Forest algorithm. Remote Sens. Environ. 231, 111234.
Wu, W., Huang, J., Cui, K., Nie, L., Wang, Q., Yang, F., Shah, F., Yao, F., Peng, S., 2012. Sheath blight reduces stem breaking resistance and increases lodging susceptibility of rice plants. F. Crop. Res. 128, 101–108.
Wu, W., Ma, B.L., Fan, J.J., Sun, M., Yi, Y., Guo, W.S., Voldeng, H.D., 2019. Management of nitrogen fertilization to balance reducing lodging risk and increasing yield and protein content in spring wheat. F. Crop. Res. 241, 107584.
Yan, W., Zhang, Y., Yang, T., Liu, X., 2019. A microwave scattering model for simulating the C-band SAR backscatter of wheat canopy. Am. J. Remote Sens. 7, 13–24.
Zhang, L., Zhang, Z., Luo, Y., Cao, J., Tao, F., 2020. Combining optical, fluorescence, thermal satellite, and environmental data to predict county-level maize yield in China using machine learning approaches. Remote Sens. 12, 21.